Effects of intracavity dispersion on the starting dynamics of continuous-wave passively mode-locked Ti:sapphire/DDI lasers

Jia-Min Shieh, Hwa-Ming Twu, and Ci-Ling Pan

Institute of Electro-Optical Engineering, National Chiao Tung University, Hsinchu, Taiwan 30010

Through analysis of transient autocorrelation traces, we show that intracavity dispersion significantly affects the number of initially oscillating modes as well as the buildup of passive mode locking in picosecond and femtosecond lasers. © 1996 Optical Society of America

In the past few years, a number of studies have analyzed theoretically both steady-state operation and self-starting conditions for passively mode-locked solid-state lasers.[1–5] These studies have focused on the mode-locking threshold and parameters of the initial fluctuation necessary to initiate mode-locking. Quantitatively, an initial fluctuation will evolve into a steady-state mode-locked pulse if and only if[1,6]

$$\kappa \overline{P}(0) > \frac{1}{\ln(m_i)} \frac{T_r}{T_c} . \tag{1}$$

In inequality (1), κ is the mode-locking strength parameter. $\overline{P}(0)$ is the power of the slowly varying average background radiation in the cavity. It is related to the peak intensity of the initial fluctuation, $\overline{p}(0) \approx \overline{P}(0) \ln(m_i)$, where m_i represents the number of initially oscillating modes. T_r and T_c are the round-trip time of the cavity and the effective mode-correlation time, respectively. The latter is defined by the inverse 3-dB full width of the first beat note of the free-running laser, $\Delta\nu_{3\mathrm{dB}}$. It is commonly assumed that the frequency-pulling effect that is due to intracavity dispersion does not significantly affect the buildup of passive mode locking. This assumption is, however, based on a guess as to the characteristic duration of the initial mode-beating fluctuations in the free-running laser, $\tau_i = T_r/m_i$. In the literature τ_i is usually estimated to be of the order of 10 ps or longer. To our knowledge, neither τ_i nor m_i was determined experimentally previously. On the other hand, modulation instability resulting from the interplay of self-phase modulation and negative dispersion can increase $\overline{p}(0)$ and facilitate the startup. This was confirmed for a Michelson additive-pulse mode-locked Nd:phosphate glass laser. Krausz *et al.*[6] showed that the intracavity threshold power for startup of this laser is $P_{\mathrm{th}} \approx 0.6$ W and $P_{\mathrm{th}} = 0.2$ W for positive and negative group-delay dispersion, respectively.

In this Letter we show that intracavity dispersion significantly affects the number of initially oscillating modes as well as the buildup of passive mode locking in picosecond and femtosecond Ti:sapphire/DDI lasers. This is achieved through analysis of transient autocorrelation traces $\Gamma(\tau_d)$ and of the spectra of the laser output as a function of delay time τ_d with respect to the

laser onset. During the pulse-formation stage, $\Gamma(\tau_d)$ exhibits a coherent spike residing on a broad shoulder. The width of the spike corresponds to the coherence time of the laser,[7] $\Delta t \approx 1/\Delta\omega$, where $\Delta\omega$ is the laser oscillating bandwidth. It also reveals the unclean appearance of the laser output, that is, a burst of light with numerous picosecond substructures on it.[7–9] The width of the shoulder, on the other hand, corresponds to the number of phase-locked modes at a particular delay time. As the laser evolves to the steady state, the contrast ratio (R is the peak-to-shoulder-height ratio) of the transient autocorrelation trace evolves from 2:1 to 2:0. The former ratio corresponds to that of a multimode randomly phased cw laser. The latter corresponds to that of a completely mode-locked laser.

Our cw passively mode-locked Ti:sapphire/DDI laser ($\lambda = 770$ nm) generates ~150-fs pulses at 79.4 MHz with intracavity dispersion-compensating SF10 prism pairs.[10] Without the prisms, the steady-state laser pulse widths are in the range of 5–15 ps. This corresponds to saturable absorber dye concentrations in the range of 2×10^{-5} to 10^{-3} M. The laser employs a six-mirror cavity with 15-cm radius-of-curvature folding mirrors around a 2-cm Brewster-angle-cut Ti:sapphire crystal. It was aligned such that the Kerr-lens strength was weak ($\kappa \sim 10^{-8}$ W^{-1}) and would not self-start without the absorber dye jet. The transient autocorrelation trace $\Gamma(\tau_d)$ and the spectrum of the laser output at a delay time of τ_d with respect to the laser onset were measured with the time-gating technique.[11,12]

In Fig. 1 we show $\Gamma(\tau_d)$ at a delay of $\tau_d = 5$ μs (~380 round trips) for the dispersion-compensated cavity (steady-state pulse width $\tau \sim 150$ fs) and the cavity with the prism pair removed ($\tau \approx 10$ ps). In Fig. 2 we show $\Gamma(\tau_d)$ at a delay of $\tau_d = 30$ μs (~2300 round trips) for the above two configurations. The widths of the coherent spikes in Fig. 1 are $\Delta t \sim 1$ ps and 25 ps for the femtosecond and the picosecond cavities, respectively. The number of initially oscillating modes is then $m_i \sim 25,000$ for the dispersion-compensated cavity and 1000 for the cavity without the prism pair. In comparison, we find that $\Delta t \sim 1.3$ ps, or $m_i \sim 19,000$, for a partially compensated cavity with a steady-state pulse width $\tau \sim 230$ fs. The absorber dye concentrations, on the other hand,
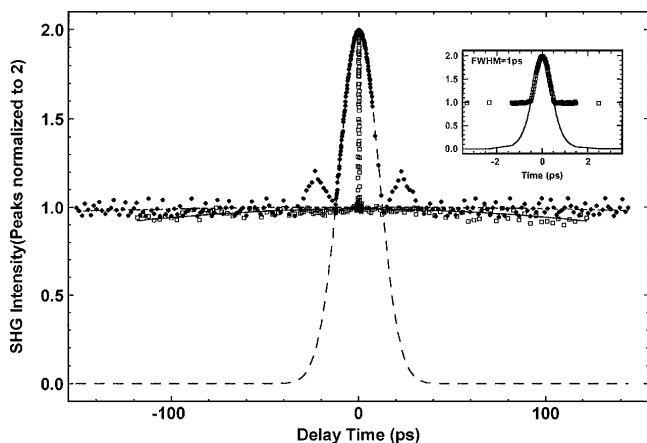
Fig. 1. Transient autocorrelation traces for the laser at $\tau_d = 5$ μs after the laser onset. The open squares and filled circles are experimental data points for the laser with and without prisms, respectively. The solid, short-dashed, and long-dashed curves are curve-fitting results for full width at half-maximum (FWHM) 880 ps, peak 0.99, with prisms; FWHM 2000 ps, peak 1, no prisms; and FWHM 25 ps, respectively. The inset shows curve fitting of the coherent spike of the trace corresponding to the femtosecond laser.

do not affect τ_c or m_i appreciably. Because the weak Kerr-lens strength is the same for all the laser configurations that we studied, clearly cavity dispersion is the dominant parameter that determines the number of initially oscillating modes. The secondary spikes located at approximately a 25-ps delay from the coherent spike peaks shown in Figs. 1 and 2 were due to the mutual correlation between side clusters of longitudinal modes. We also observed secondary spikes for a similar picosecond laser at somewhat higher absorber dye concentrations $(3 \times 10^{-4}$ M).[12]

The broad shoulder of $\Gamma(\tau_d)$ shown in Figs. 1 and 2, on which the coherent spikes ride, is related to the number of phase-locked modes at τ_d. At $\tau_d = 5$ μs and $\tau_d = 30$ μs, the shoulder widths were both ~2000 ps, corresponding to nine phase-locked modes for the picosecond laser configuration. The peak heights of the shoulders remained equal to 1. For the dispersion-compensated cavity, these widths narrowed from 880 to 400 ps, and the peak heights decreased from 0.95 to 0.86 as the laser evolved from $\tau_d = 5$–30 μs. That is, the number of phase-locked modes increased from ~20 to 45. Clearly the pulse-shaping process advanced more rapidly for the cavity with the dispersion-compensating prisms. The entire buildup process for our laser in several configurations is shown in Fig. 3, which gives the inverse contrast ratio R^{-1} as a function of delay time. For the cw laser, with or without prisms, $R^{-1} = 0.5$ throughout the buildup; this value corresponds to that for a multimode randomly phased cw laser. The value R^{-1} for the partially compensated cavity falls between curves for the cavity without the prisms and for the cavity with optimum dispersion compensation. Furthermore, pulse buildup to the steady state for the latter cavity was much faster, reaching the asymptotic value for the steady-state mode-locked pulses, $R^{-1} = 0$, in 130 μs as opposed to 220 μs for the cavity without prisms.

It is instructive to evaluate the initial pulse-shortening force power round trip, $s = 1/\tau_{\mathrm{eff}}\, \mathrm{d}\tau_{\mathrm{eff}}/\mathrm{d}n$, for different laser configurations. Here $\tau_{\mathrm{eff}} = \tau_{\mathrm{ss}}(\overline{p}_\omega/\overline{p}_\omega{}^{\mathrm{ss}})^2/(\overline{p}_{2\omega}/\overline{p}_{2\omega}{}^{\mathrm{ss}})$ is the effective pulse width of the laser output at a given delay time.[13] The parameters $\overline{p}_\omega$ and $\overline{p}_{2\omega}$ are transient fundamental and second-harmonic-generated laser power, respectively, and τ_{ss}, $\overline{p}_\omega{}^{\mathrm{ss}}$, and $\overline{p}_{2\omega}{}^{\mathrm{ss}}$ are steady-state values of the laser pulse width, fundamental, and second-harmonic generated power, respectively. We have also calculated the transient pulse width, fundamental, and second-harmonic-generated power by numerically solving Haus's master equation of mode locking[14] in a manner similar to that of Kärtner and Keller.[15] For the initial field envelope, however, we assume a Gaussian distribution of randomly phased modes, the
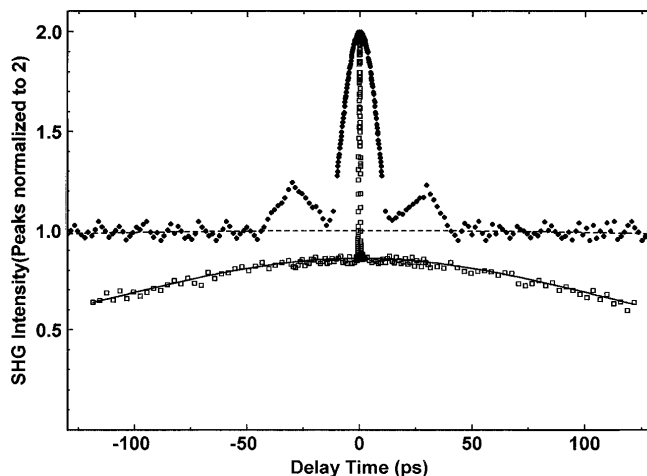

Fig. 2. Transient autocorrelation traces for the laser at $\tau_d = 30$ μs after the laser onset. The open squares and filled circles are experimental data points for the laser with and without prisms. The solid curve and the dashed line are curve-fitting results for the shoulders of the autocorrelation traces for the above two cases, respectively. For the solid curve, FWHM 400 ps and peak 0.86, and for the dashed line, FWHM 2000 ps and peak 1.0.
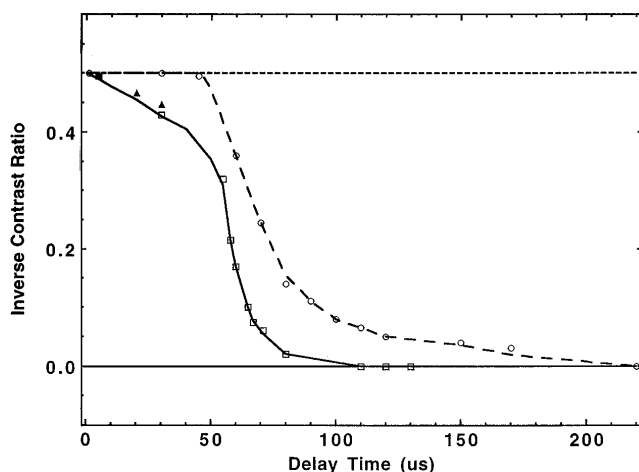

Fig. 3. Inverse contrast ratios R^{-1} for the laser in several configurations are plotted as a function of delay time after the laser onset: solid curve, with prisms; short-dashed curve, cw (with or without prisms); long-dashed curve, without prisms; ▲, partially compensated. The shapes are data points.

number of which was experimentally determined from the coherent spikes of the transient autocorrelation traces. At an absorber concentration of 5×10^{-5} M, we calculated that $s = -6.0 \times 10^{-5}$ for the picosecond cavity ($D = 1250 \, \text{fs}^2$) and $s = -1.0 \times 10^{-4}$ for the dispersion-compensated cavity ($D = -3000 \, \text{fs}^2$). This is consistent with our experimental observations described above. On the other hand, the Kerr-lens strength is the same for both configurations, $\kappa \approx 2.0 \times 10^{-8} \, \text{W}^{-1}$. The corresponding pulse-shortening force $s_\kappa = -2.0 \times 10^{-6}$. In comparison, we estimate that $\kappa = 1.0 \times 10^{-7} \, \text{W}^{-1}$ and $s_\kappa = -1.0 \times 10^{-5}$ for a self-starting Kerr-lens mode-locked Ti:sapphire laser.[16] Significantly, this is comparable in magnitude with the dispersion-related pulse-shortening force. Following Agrawal[17] and Krausz *et al.*[6] we note that, for the modulation instability that is necessary to initiate self-starting, the optimum group-delay dispersion for the cavity must be $|D_{\text{opt}}| = 2\phi \overline{P}(0)/\Delta\nu_i{}^2$. With the self-phase modulation strength $\phi = 2.0 \times 10^{-6} \, \text{W}^{-1}$, $\overline{P}(0) = 10$ W, the free-running laser line width $\Delta\nu_i = 6.0 \times 10^{11} \, \text{s}^{-1}$, and $|D_{\text{opt}}| = 100 \, \text{fs}^2$. This is substantially smaller than the group-delay dispersion in our femtosecond cavity. Nonetheless, the dispersion effect on the starting dynamics was already observable in this study. State-of-the-art Kerr-lens mode-locked Ti:sapphire lasers,[18] however, employ a cavity with near-zero second- and third-order dispersion. We therefore predict that dispersion will play a significant role in the starting dynamics of this class of lasers.

In summary, we show that intracavity dispersion is the dominant physical parameter that determines the number of initially oscillating modes in a passively mode-locked Ti:sapphire laser. Our results also suggest that dispersion, probably in combination with self-phase modulation, plays an important role as a pulse-shortening force in the starting dynamics.

References

1. F. Krausz, T. Brabec, and Ch. Spielmann, Opt. Lett. **16,** 235 (1991).
2. H. A. Haus and E. P. Ippen, Opt. Lett. **16,** 1331 (1991).
3. J. Hermann, J. Opt. Soc. Am. B **11,** 496 (1994).
4. S. Chen and J. Wang, Opt. Lett. **16,** 1689 (1991).
5. C.-J. Chen, P. K. A. Wai, and C. R. Menyuk, Opt. Lett. **20,** 350 (1995).
6. F. Krausz, M. E. Fermann, T. Brabec, P. F. Curley, M. Hofer, M. H. Ober, C. Spielmann, E. Wintner, and A. J. Schmidt, IEEE J. Quantum Electron. **23,** 2097 (1992).
7. D. J. Bradley and G. H. C. New, Proc. IEEE **62,** 313 (1974).
8. H. A. Pike and M. Hercher, J. Appl. Phys. **41,** 4562 (1970).
9. M. A. Duguay, J. W. Hansen, and S. L. Shapiro, IEEE J. Quantum Electron. **QE-6,** 49 (1970).
10. C.-L. Pan, C.-D. Hwang, J.-C. Kuo, J.-M. Shieh, and K.-H. Wu, Opt. Lett. **17,** 1445 (1992).
11. J.-C. Kuo, J.-M. Shieh, C.-D. Hwang, C.-S. Chang, and C.-L. Pan, Opt. Lett. **17,** 334 (1992).
12. N.-W. Pu, J.-M. Shieh, Y. Lai, and C.-L. Pan, Opt. Lett. **20,** 163 (1995).
13. Y. C. Chen and J. M. Liu, Appl. Phys. Lett. **47,** 602 (1985).
14. H. A. Haus, J. Appl. Phys. **46,** 3049 (1975).
15. F. X. Kärtner and U. Keller, Opt. Lett. **20,** 16 (1995).
16. J.-M. Shieh, F. Ganikhanov, K.-H. Lin, W.-F. Hsieh, and C.-L. Pan, J. Opt. Soc. Am. B **12,** 945 (1995).
17. G. P. Agrawal, *Nonlinear Fiber Optics* (Academic, New York, 1989).
18. J. Zhou, G. Taft, C.-P. Huang, M. M. Murnane, and H. C. Kapteyn, Opt. Lett. **19,** 1149 (1994).